Characterization of a gated fiber-optic-coupled detector for application in clinical electron beam dosimetry

James A. Tanyi[a)]
Department of Radiation Medicine, Oregon Health and Science University, Portland, Oregon 97239 and Department of Nuclear Engineering and Radiation Health Physics, Oregon State University, Corvallis, Oregon 97331

Kevin D. Nitzling and Camille J. Lodwick
Department of Nuclear Engineering and Radiation Health Physics, Oregon State University, Corvallis, Oregon 97331

Alan L. Huston and Brian L. Justus
Optical Sciences Division, Naval Research Laboratory, Washington, DC 20375

(Received 31 July 2010; revised 17 December 2010; accepted for publication 21 December 2010; published 28 January 2011)

Purpose: Assessment of the fundamental dosimetric characteristics of a novel gated fiber-optic-coupled dosimetry system for clinical electron beam irradiation.
Methods: The response of fiber-optic-coupled dosimetry system to clinical electron beam, with nominal energy range of 6–20 MeV, was evaluated for reproducibility, linearity, and output dependence on dose rate, dose per pulse, energy, and field size. The validity of the detector system's response was assessed in correspondence with a reference ionization chamber.
Results: The fiber-optic-coupled dosimetry system showed little dependence to dose rate variations (coefficient of variation $\pm 0.37\%$) and dose per pulse changes (with 0.54% of reference chamber measurements). The reproducibility of the system was $\pm 0.55\%$ for dose fractions of ~ 100 cGy. Energy dependence was within $\pm 1.67\%$ relative to the reference ionization chamber for the 6–20 MeV nominal electron beam energy range. The system exhibited excellent linear response ($R^2 = 1.000$) compared to reference ionization chamber in the dose range of 1–1000 cGy. The output factors were within $\pm 0.54\%$ of the corresponding reference ionization chamber measurements.
Conclusions: The dosimetric properties of the gated fiber-optic-coupled dosimetry system compare favorably to the corresponding reference ionization chamber measurements and show considerable potential for applications in clinical electron beam radiotherapy. [DOI: 10.1118/1.3539737]

Key words: real-time dosimetry, pulsed electron beam, gated fiber optics, *in vivo* dosimetry

I. INTRODUCTION

In vivo dosimetry plays a crucial role in radiotherapy quality assurance by allowing the assessment of random and/or systematic treatment deviations, essentially revealing uncertainties between prescribed and administered radiotherapy doses. The most commonly used *in vivo* patient dosimetry systems include thermoluminescence dosimeters (TLDs), silicon diodes, and metal oxide semiconductor field effect transistors (MOSFETs). Unlike TLDs that are not coupled to a signal processing system, diodes have the advantage of providing real-time feedback of accumulated dose. However, the response of diodes is dependent on a number of parameters, including the direction of the incident radiation, dose rate, dose per pulse, temperature, and field size,[1] each of which necessitates a corrective action. Furthermore, compensatory energy-dependent buildup layer in diode manufacturing renders them bulky to the extent that they may perturb fluences. Mitigating the drawbacks of the diode system has propelled MOSFETs (Ref. 2) into a favorable alternative for clinical radiation therapy quality assurance. However, MOSFETs have relatively short life span, exhibit directional and energy-dependent response, and also require frequent recalibration.[3–5]

To overcome the shortfalls of TLD, diode, and MOSFET dosimetry systems, a recent approach to *in vivo* dosimetry involves the utilization of ultrasmall probes consisting of near tissue-equivalent plastic scintillators connected to optical fibers.[6–9] In addition to their good spatial and temporal resolution, scintillation detectors have favorable radiation response characteristics that include reproducibility, linearity of response with dose, dose-rate proportionality, and energy independence when compared to other more commonly used detector systems. Nonetheless, these detectors have not realized their full potential for routine clinical applications in radiation oncology due mainly to the limitations imposed by signal coupling inefficiencies and noise capture. Because dark current input to total noise is negligible, the main contribution to the aforementioned limitations thus arises from radiation-induced light produced in the optical fibers due to a combination of Cerenkov emission and native fluorescence or luminescence, depending on the type of material used for the fibers.[6]

Cerenkov radiation is generated in optical fibers when

charged particles enter the core with a velocity (c/n, where c is the speed of light in a vacuum and n is the refractive index of the core material) greater than the local speed of light. Since Cerenkov radiation is created by charged particles, the amount of Cerenkov radiation produced by an electron beam will be significantly larger than that produced by a photon beam. For example, for 6 MeV and 12 MeV electrons beams, the maximum Cerenkov contribution compared to the light output produced by a small-sized pure fused silica scintillator is of the order of ~12% and occurs when exposed at the depths of maximum dose of the respective electron energies in a 10×10 cm^2 field size.[10] The intensity of the radiation is strongly dependent on the angle between the optical fiber axis and the particle trajectory, reaching a maximum when the Cerenkov cone is directed along the fiber axis. While Cerenkov radiation is not directly related to the radiation dose to the scintillator,[11,12] its magnitude can exceed the intensity of the scintillation signal even at a wavelength where the scintillation light is at its most intense. Thus, for accurate dosimetric measurements, the Cerenkov radiation must be removed from the scintillation signal.

Different methods have been proposed and tested to correct for the effects of Cerenkov radiation on scintillation dosimetry. Beddar *et al.*[10] used a "background fiber" immediately adjacent to a signal fiber to perform background subtraction of Cerenkov radiation from the scintillation signal. This technique, nevertheless, is limited by a potential disparity in background signal generation in each fiber, particularly in high dose gradient regions. de Boer *et al.*[13] exploited spectral differences between scintillation light from a long wavelength emitting scintillator and Cerenkov radiation to reduce, but not eliminate, the interference caused by the Cerenkov radiation. Fontbonne *et al.*[14] used a technique known as chromatic filtration to again reduce, but not eliminate, the Cerenkov background signal. Because linear-accelerator-based radiotherapy beams are pulsed, scintillation signals may be resolved temporally from the prompt Cerenkov and native luminescent radiation if the relaxation time of the scintillator is long enough and the dose delivered by the radiotherapy unit between pulses is negligible. To obtain scintillation signals alone, the time interval when sampling occurs is selected such that it is after the termination of the signal induced by Cerenkov radiation and native luminescence and before the termination of scintillation signals; a gating concept exploited by both Clift *et al.*[15] and Justus *et al.*[16] However, unlike Clift *et al.*[15] who used a plastic scintillator with relatively shorter emission times as the radiation-sensitive material, Justus *et al.*[16] used copper ion (Cu^+)-doped quartz with relatively longer luminescence decay times; hence, a more effective means of temporally resolving scintillation signals from Cerenkov radiation and native luminescence.

The gated Cu^+-doped quartz optical fiber dosimeter[16–19] is examined for clinical applications in the current study. Benevides *et al.*[20] has assessed its performance for use in mammography energy range, Hyer *et al.*[21] in diagnostic radiology, and Tanyi *et al.*[5] in the therapeutic photon radiation realm. In this study, a systematic investigation of its fundamental response characteristics to clinical radiotherapy electron beams is presented.

II. MATERIALS AND METHODS

II.A. Gated fiber-optic-coupled dosimeter

The principle of operation of the gated fiber-optic-coupled dosimeter (FOCD) used in the current study has been described elsewhere.[5,16] In brief, the radiation-sensitive portion of the fiber dosimeters consists of a 1 mm length of Cu^+-doped fused quartz fiber fusion-spliced to one end of a 1 m long, multimode optical fiber. The diameter of the Cu^+-doped fused quartz fiber (0.4 mm) is equal to that of the silica glass core of the multimode fiber. The multimode fiber is clad with silicone and a black Tefzel jacket to ensure light tightness. The luminescence signal from the Cu^+-doped fused quartz is transmitted down the multimode optical fiber to a 15-m-long fiber-optic patch cord for readout outside the treatment room. The readout unit used for the current study is equipped with three separate channels permitting simultaneous measurement of signals from three dosimeter fibers. The readout unit uses three photon counting photomultiplier tube modules (model HC124-03, Hamamatsu Corporation, Bridgewater, NJ) to detect the luminescence signal in each of the three optical fiber dosimeters. The Cu^+-doped luminescence signal in each fiber dosimeter is separated from Cerenkov radiation and native luminescence generated in the silica multimode fiber by using a software gating method. Originally, gate synchronization signal was provided by an electronic sync pulse taken from the power supply of a medical linear accelerator (linac).[16,19] However, due to variations in the polarity, magnitude, and overall quality of the electronic sync pulses as a function of the individual linac unit, the electronics in the dosimeter had to be modified for each machine. In order to provide a gate synchronization signal that could be used universally, a scattered-photon trigger detector,[5] consisting of a block of plastic scintillator (Saint-Gobain BC-408) having dimensions of ~10 cm$\times$2.5 cm $\times$2 cm, edge-coupled directly to the face of a photomultiplier tube module (model HC124-03, Hamamatsu Corporation, Bridgewater, NJ), was used. The scattered-photon trigger detector was placed on a wall in the treatment room, ~4 m from the radiation source. All other features of the gated optical fiber dosimeter system, including the software and data acquisition procedures, have been described in some detail previously.[16] Briefly, the output pulses from the single photon counting module were collected by a 32-bit counter configured to collect the data in a semiperiod buffered counting mode. The counter sum was transferred into a buffer on both the rising and the falling edges of each gate pulse from the scattered-photon trigger. The signal collected during the gate pulse includes the Cerenkov background as well as native fiber luminescence, while the signal collected between pulses corresponds to the Cu^+-doped luminescence signal. An 80 MHz clock was used in conjunction with an additional 32 bit counter to accurately measure the duration of each gate pulse and the interval between pulses. After

subtracting the photomultiplier tube dark noise, the accumulated dose and the dose rate were calculated and presented in near-real time.

II.B. Reference dosimetry

Three FOCDs were used in the current study. A 0.6 cm^3 PTW N30004 ionization chamber with graphite wall with thickness of 0.079 g/cm^2, an inner aluminum electrode of 1.0 mm diameter, and an air cavity radius of 0.305 cm, interfaced with a PTW UNIDOS E electrometer (Physikalisch-Technische Werkstaetten, Freiburg, Germany), was used to provide reference dosimetry to quantitate the validity of the FOCD response. The calibration of the reference ionization chamber and electrometer combination is traceable to an Accredited Dosimetry Calibration Laboratory (ADCL).

II.C. Linear accelerator

A Varian Trilogy treatment platform (Varian Medical Systems, Palo Alto, CA), capable of producing electron beams with nominal energies of 6, 9, 12, 16, and 20 MeV, was used in the current study. This treatment unit is also equipped with electron collimation (cone) applicators with dimensions of 6×6, 10×10, 15×15, 20×20, and 25×25 cm^2.

II.D. Phantom and measurement standardization

Measurements were performed in a $30\times30\times16.5$ cm^3 Plastic Water® phantom (CNMC Co., Inc., Nashville TN) with slabs of varying thickness. Unless otherwise stated, measurements were performed at standard calibration setup; that is, source-to-surface distance (SSD) of 100 cm, cone size of 10×10 cm^2 at SSD, nominal gantry angle of 0° (International Electrotechnical Commission or IEC standards), and depth of maximum dose (1.2 cm for 6 MeV, 2.0 cm for 9 MeV, 3.0 cm for 12 MeV, 3.0 cm for 16 MeV, and 3.0 cm for 20 MeV) as the point of measurement. With each dosimeter centered on the central axis of the treatment unit beam port, the nominal delivered dose was 1 cGy for every 1 monitor unit (MU) of radiation. Finally, for all the experiments except for reproducibility measurements and unless otherwise stated, the response of each FOCD was computed as an average of five sequential readings, delivered and recorded at a machine dose rate of 600 MU/min.

II.E. Dose-rate and dose per pulse dependence

The FOCDs were irradiated with the 6 MeV electron beam using the standard calibration configuration to investigate the dependence of their response on machine dose rate. Dose-rate response dependence was assessed for the following machine settings: 100, 200, 300, 400, 500, 600, and 1000 MU/min. For each dose rate, a reading corresponding to 100 MU at the standard calibration position was recorded and the results were normalized to the response at 600 MU/min for postexposure computation of a coefficient of variation (COV). The dose per pulse (that is, the product of the pulse width and the instantaneous dose rate) response dependence of the FOCDs was also assessed for the 6 MeV beam energy by changing the SSD from 100 to 125 cm, in 5 cm increments, and the recorded readings normalized to the reading at 100 cm SSD. Corresponding measurements were also performed with the reference ionization chamber.

II.F. Reproducibility

For each available electron energy, the FOCDs were repeatedly irradiated at standard calibration setting and 600 MU/min dose rate to 100 MU 25 times. The mean of each 25 consecutive readings was found, and the percentage difference between each consecutive reading and its corresponding mean was calculated. A COV was also calculated and used to define the dosimetry system's reproducibility.

II.G. Energy dependence

Energy dependence was evaluated by computing the ratio of the integrated scintillation output of each FOCD at a specified depth and at depth of maximum dose for a 10×10 cm^2 cone size and 100 cm SSD. For the purpose of this study, the specified depths were 2.0 cm for 6 MeV, 3.0 cm for 9 MeV, 4.0 cm for 12 MeV, 5.5 cm for 16 MeV, and 6.5 cm for 20 MeV. Corresponding ratios, termed ionization ratios, were also computed for the reference ionization chamber.

II.H. Linearity

To identify the useful dynamic range of the dosimetry system and to ensure that the scintillator output is free from any fatigue effect for the relatively short exposure times and accumulated doses typical of the useful dynamic range, linearity measurements were performed on the FOCDs across a range of potential clinical doses for each of the available electron energies. The delivered doses ranged from machine settings of 1 to 1000 MU and measurements were normalized to the reading at 100 MU and compared to similar reference ionization chamber measurements.

II.I. Field size dependence

Fiber-optic-coupled dosimeter field size response dependence was performed at standard calibration setup, except for the electron cone applicator dimension that was variable, and

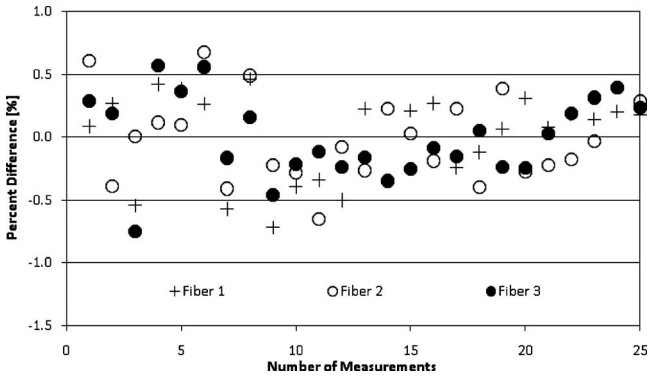

FIG. 1. Reproducibility of 100 cGy dose fractions from the 6 MeV beam.

TABLE I. Percentage standard deviations for signal relative to the average readings.

Energy (MeV)	Fiber 1	Fiber 2	Fiber 3
6	0.35	0.35	0.32
9	0.41	0.35	0.55
12	0.34	0.40	0.34
16	0.37	0.40	0.40
20	0.27	0.23	0.28

reported as output factors. Thus, for each of the available electron energies, the FOCD readings for different cones were recorded and normalized to the reading for the 10 $\times$10 cm^2 cone. Corresponding measurements were also performed for the reference ionization chamber.

III. RESULTS

III.A. Reproducibility

Figure 1 shows the percent deviation of 25 sequential FOCD signals from their mean value as a response to 100 cGy dose fractions from the 6 MeV electron beam energy. The reproducibility of the FOCD system was within $\pm$0.55% (Table I).

III.B. Linearity

The response of the FOCD system was in excellent agreement with reference ionization chamber measurements for low dose (that is, 1–10 cGy) and high dose (that is, 11–1000 cGy) ranges for nominal electron beam energies in the range of 6–20 MeV [see Figs. 2(a) and 2(b) for the 6 MeV beam energy]. The dose response of the FOCD system for all electron energies was linear; the linear regression correlation coefficients (R^2) were found to be equal to 1.000.

III.C. Dose rate and dose per pulse dependence

Figure 3 shows the average dose rate dependence of the FOCD system at dose rates ranging from 100 to 1000 MU/min. The FOCD response was within $\pm$0.50% of the reference ionization chamber measurements and remained uniform well within the reproducibility of the FOCD system. Figure 4 shows the relative response of the FOCDs and the reference ionization chamber plotted against SSDs ranging from 100 to 125 cm for the 6 MeV electron beam. The FOCD response was within $\pm$0.54% of the reference ionization chamber measurements.

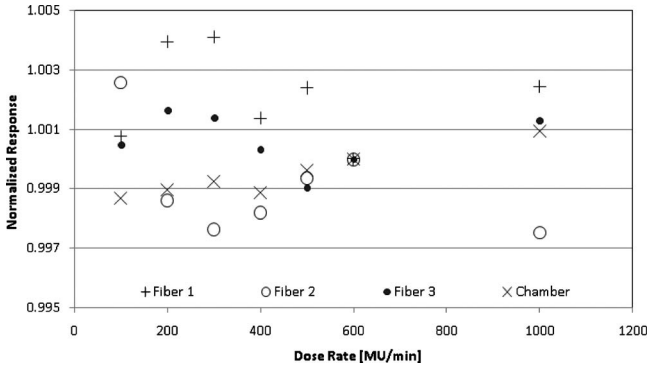

FIG. 3. Dose-rate response of three FOCDs and a reference ionization chamber under pulsed radiation from the 6 MeV electron beam. Dose-rate response was normalized to unity by the response at 600 MU/min.

III.D. Field size dependence

Table II shows a comparison of the output factors measured with each FOCD and the reference ionization chamber. The FOCD output factors were in good agreement with those of the reference ionization chamber. Quantitatively, the maximum difference between the FOCD response and that of the reference ion chamber was within $\pm$0.54% (6 MeV), $\pm$0.35% (9 MeV), $\pm$0.50% (12 MeV), $\pm$0.42% (16 MeV), and $\pm$0.48% (20 MeV).

III.E. Energy dependence

Figure 5 shows the energy response of the FOCD system for clinical electron beams in the range of 6–20 MeV. The ratio of each FOCD's integrated scintillation output at a

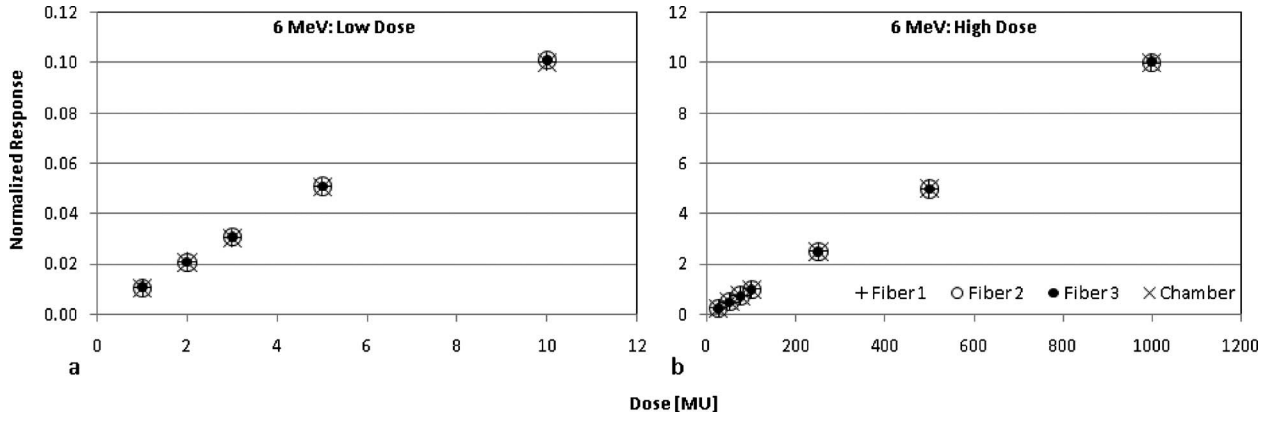

FIG. 2. Response curves of three FOCDs and a reference ionization chamber for (a) low doses (range: 1–10 cGy) and (b) high doses (range: 11–1000 cGy) for the 6 MeV beam, measured at standard calibration settings; the linearity coefficient R^2 is 1.000 for the FOCDs.

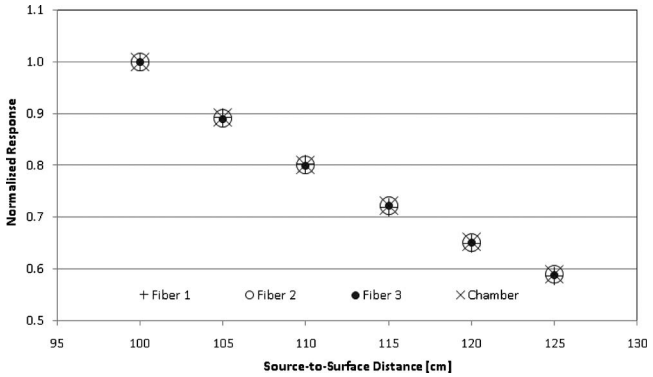

FIG. 4. Dose per pulse response of three FOCDs and a reference ionization chamber under pulsed radiation from the 6 MeV electron beam. Dose per pulse response was normalized to unity by the response at 100 cm source-to-surface distance.

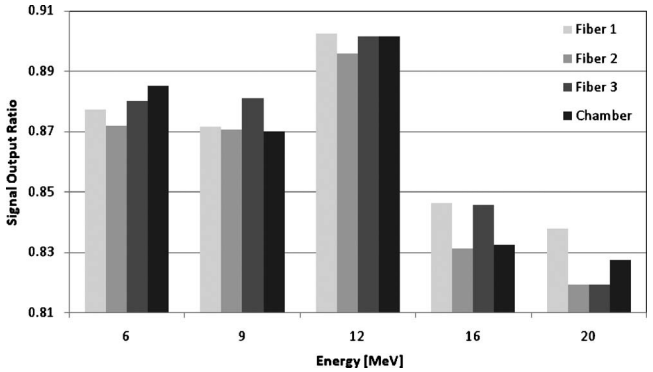

FIG. 5. Energy response of four detectors: Three FOCDs and a reference ionization chamber. Energy response was computed as the ratio of each detector's signal output at two depths; a specified depth and at depth of maximum dose, for a 10×10 cm^2 cone size and 100 cm SSD.

specified depth to that at depth of maximum dose for a 10×10 cm^2 cone size and 100 cm SSD correlated well with the corresponding reference ionization chamber ionization ratio and was within $\pm1.67\%$ for all the energies investigated, indicating little or no energy dependence.

IV. DISCUSSION

In the current study, the characteristics of the Cu^+-doped scintillation detector for clinical electron beams with nominal energy in the range of 6–20 MeV are assessed. The output of a linear accelerator is a train of pulses, each typically ~5 μs wide. The pulse repetition rate varies between ~50 and ~600 Hz; as such, the time interval between electron pulses varies from ~20 ms (corresponding to the machine dose rate of 100 MU/min) to ~2 ms (corresponding to the machine dose rate of 1000 MU/min). During each electron pulse, the signal from each dosimeter fiber includes scintillation from the Cu^+-doped fiber sensor plus Cerenkov radiation and native luminescence from all portions of the multimode fiber exposed to the electron beam. The decay of the Cerenkov emission is on the order of a picosecond, while the native fluorescence decays on a nanosecond time scale; hence, both the Cerenkov and the native luminescence emissions are immediately terminated after the electron pulse terminates. In contrast, the luminescence signal from the Cu^+-doped glass persists for several hundred microseconds

TABLE II. Output factors measured with a reference ionization chamber and three fiber-optic-coupled dosimeters in a solid water phantom. FOCD is fiber-optic coupled dosimeter.

Energy (MeV)	Dosimeter	Field size (cm^2)				
		6	10	15	20	25
6	Chamber	0.966	1.000	1.003	1.014	1.010
	Fiber 1	0.961	1.000	0.998	1.012	1.009
	Fiber 2	0.970	1.000	1.004	1.009	1.006
	Fiber 3	0.969	1.000	1.001	1.009	1.005
9	Chamber	0.978	1.000	0.997	0.984	0.963
	Fiber 1	0.979	1.000	0.998	0.985	0.963
	Fiber 2	0.981	1.000	0.998	0.984	0.962
	Fiber 3	0.982	1.000	0.995	0.983	0.960
12	Chamber	0.968	1.000	0.993	0.976	0.949
	Fiber 1	0.971	1.000	0.995	0.980	0.952
	Fiber 2	0.974	1.000	0.994	0.974	0.949
	Fiber 3	0.972	1.000	0.988	0.973	0.949
16	Chamber	0.985	1.000	0.986	0.970	0.939
	Fiber 1	0.988	1.000	0.986	0.973	0.943
	Fiber 2	0.989	1.000	0.987	0.966	0.942
	Fiber 3	0.988	1.000	0.985	0.968	0.937
20	Chamber	0.999	1.000	0.978	0.955	0.923
	Fiber 1	0.999	1.000	0.977	0.959	0.928
	Fiber 2	1.002	1.000	0.973	0.954	0.923
	Fiber 3	1.001	1.000	0.981	0.959	0.923

after the electron pulse terminates. Because of the differences in these lifetimes, the signal due to Cerenkov radiation and the native luminescence is efficiently separated from the scintillation signal between electron pulses by gated detection.[16] Since the scintillation signal is measured after each individual electron pulse, the measurements and the dose response are expected to be independent of the dose rate (Fig. 3). The observed results confirm this expectation, also indicating that no ion-recombination effect exists in the FOCD system. Hence, no correction is needed for the FOCD reading while changing the dose rate between 100 and 1000 MU/min. In addition to changes in machine dose rate, SSD variation can, in effect, also introduce a change in the dose per pulse at a point of interest. The results in the current study also indicate that the FOCD response is independent of dose per pulse changes as a function of SSD variation (Fig. 4).

The reproducibility of the scintillation detector under electron irradiation was examined at 600 MU/min with each measurement representing the integrated signal obtained from an irradiation of 100 MU at standard calibration setting. The percentage standard deviations of the recorded signals are contained well within a 0.55% envelope relative to the average reading (Fig. 1 and Table I).

The gated measurement of scintillation light generated by the Cu^+-doped quartz dosimeter will be a direct measure of dose only if the quartz has (1) high ionizing radiation sensitivity and scintillation efficiency (that is, the fraction of the electron kinetic energy converted into detectable fluorescent light is large and is independent of the energy of the charged particle) and (2) high transparency to the scintillation light. As such, the light emitted should have a linear dependence on the energy deposited by the charged particles interacting within the detector. In the current study, it was demonstrated that the conversion is linear with a proportional light yield to deposited energy over a dose range of 1–1000 cGy for electron energies in the range of 6–20 MeV [see Figs. 2(a) and 2(b) for the 6 MeV beam energy].

Despite an effective atomic number of ~10.8 and a density of 2.2 g/cm^3, Cu^+-doped fused quartz, composed primarily of silica (99.7%), showed no observable energy response dependence in the range of 6–20 MeV (Fig. 5), attributable in part to the constancy of the water-to-silica collision mass stopping power ratios in the electron energy range assessed.[22] Hence, no energy correction should be necessary while performing *in vivo* measurements.

Finally, cone sizes ranging from 6×6 to 25×25 cm^2 were used to investigate the influence of a potential "stem effect" caused by fluorescence/Cerenkov radiation generated during electron beam irradiation. For each field size, the FOCDs were placed on the central axis of the beam. Thus, the length of the optical fiber that was exposed to radiation varied from 3 cm (for the 6×6 cm^2 cone) to 12.5 cm (for the 25×25 cm^2 cone). Because Cerenkov radiation is generated only in that portion of the optical fiber that is exposed to radiation, the Cerenkov interference is expected to increase as the field size increases. The gated signal outputs of the FOCDs as a function of field (cone) size, compared to the corresponding measurements from the reference ionization chamber, are shown in Table II. There is excellent agreement between the gated signal output of the FOCDs and the reference ionization chamber output for all cone sizes investigated, indicating efficient separation of Cerenkov radiation and native luminescence from scintillation signal by gated detection.

IV.A. Limitations

Long-term stability and changes in response due to radiation damage are beyond the scope of the current study and are not examined. Regarding directional response dependence, the work of Benevides *et al.*[20] has shown that the FOCD axial-angular response is nearly uniform without any marked variations in sensitivity. This is in conformity with the $\leq$2% uniform directional response reported by Miller *et al.*.[23] for therapeutic photon and electron energies. Like Miller *et al.*,[23] Benevides *et al.*[20] also showed that the FOCD tilt or normal-to-axial-angular response exhibited a marked decrease in sensitivity along the long axis of the detector, which is attributed to (1) photon attenuation in the length of the optical fiber connecting the dosimeter to the photodetector and (2) decrease in cross-sectional area of the sensitive element presented to the incident beam stemming from the fact that the sensitive element of the FOCD is homogeneous and cylindrically symmetric. As a result of these findings, directional response dependence is beyond the scope of the current study.

V. CONCLUSION

The Cu^+-doped quartz dosimeter has demonstrated reproducible dose measurements of electron beams with a linear response to absorbed dose and response independent of dose rate, dose per pulse, and energy. This performance is achieved by gating the detection of the scintillation signal with each electron pulse, thereby effectively eliminating the background signal due to Cerenkov radiation.

[a]Author to whom correspondence should be addressed. Electronic mail: tanyij@ohsu.edu

[1]AAPM, "Diode in vivo dosimetry for patients receiving external beam radiation therapy," AAPM Report No. 87 (American Association of Physicists in Medicine, College Park, MD, 2005).
[2]I. Thomson, R. E. Thomas, and L. P. Berndt, "Radiation dosimetry with MOS sensors," Radiat. Prot. Dosim. **6**, 121–124 (1984).
[3]R. Ramani, S. Russell, and P. O'Brien, "Clinical dosimetry using MOSFETs," Int. J. Radiat. Oncol., Biol., Phys. **37**, 959–964 (1997).
[4]T. Cheung, M. J. Butson, and P. K. Yu, "Energy dependence corrections to MOSFET dosimetric sensitivity," Australas. Phys. Eng. Sci. Med. **32**, 16–20 (2009).
[5]J. A. Tanyi, S. P. Krafft, T. Hagio, M. Fuss, and B. J. Salter, "MOSFET sensitivity dependence on integrated dose from high-energy photon beams," Med. Phys. **35**, 39–47 (2008).
[6]A. S. Beddar, T. R. Mackie, and F. H. Attix, "Cerenkov light in optical fibers and other light pipes irradiated by electron beams," Phys. Med. Biol. **37**, 925–935 (1992).
[7]R. Gaza, S. W. S. McKeever, M. S. Akselrod, A. Akselrod, T. Underwood, C. Yoder, C. E. Andersen, M. C. Aznar, C. J. Marckmann, and L. Bøtter-Jensen, "A fiber-dosimetry method based on OSL from Al2O3:C for radiotherapy applications," Radiat. Meas. **38**, 809–812 (2004).
[8]M. C. Aznar, C. E. Andersen, L. Botter-Jensen, S. Å. J. Bäck, S. Mattsson, F. Kjær-Kristoffersen, and J. Medin, "Real-time optical-fibre lumi-

nescence dosimetry for radiotherapy: Physical characteristics and applications in photon beams," Phys. Med. Biol. **49**, 1655–1669 (2004).
[9]R. Gaza and S. W. McKeever, "A real-time, high-resolution optical fibre dosimeter based on optically stimulated luminescence (OSL) of KBr:Eu, for potential use during the radiotherapy of cancer," Radiat. Prot. Dosim. **120**, 14–19 (2006).
[10]A. S. Beddar, T. R. Mackie, and F. H. Attix, "Water-equivalent plastic scintillation detectors for high-energy beam dosimetry: II. Properties and measurements," Phys. Med. Biol. **37**, 1901–1913 (1992).
[11]S. H. Law, S. C. Fleming, N. Suchowerska, and D. R. McKenzie, "Optical fiber design and the trapping of Cerenkov radiation," Appl. Opt. **45**, 9151–9159 (2006).
[12]S. H. Law, N. Suchowerska, D. R. McKenzie, S. C. Fleming, and T. Lin, "Transmission of Cerenkov radiation in optical fibers," Opt. Lett. **32**, 1205–1207 (2007).
[13]S. F. de Boer, A. S. Beddar, and J. A. Rawlinson, "Optical filtering and spectral measurements of radiation induced light in plastic scintillation dosimetry," Phys. Med. Biol. **38**, 945–958 (1993).
[14]J. M. Fontbonne, G. Iltis, G. Ban, A. Battala, J. C. Vernhes, J. Tillier, N. Bellaize, C. Le Brun, B. Tamain, K. Mercier, and J. C. Motin, "Scintillating fiber dosimeter for radiation therapy accelerator," IEEE Trans. Nucl. Sci. **49**, 2223–2227 (2002).
[15]M. A. Clift, P. N. Johnston, and D. V. Webb, "A temporal method of avoiding the Cerenkov radiation generated in organic scintillator dosimeters by pulsed mega-voltage electron and photon beams," Phys. Med. Biol. **47**, 1421–1433 (2002).
[16]B. L. Justus, P. Falkenstein, A. L. Huston, M. C. Plazas, H. Ning, and R. W. Miller, "Gated fiber-optic-coupled detector for in vivo real-time radiation dosimetry," Appl. Opt. **43**, 1663–1668 (2004).
[17]A. L. Huston, B. L. Justus, P. L. Falkenstein, R. W. Miller, H. Ning, and R. Altermus, "Remote optical fiber dosimetry," Nucl. Instrum. Methods Phys. Res. B **184**, 55–67 (2001).
[18]A. L. Huston, B. L. Justus, P. L. Falkenstein, R. W. Miller, H. Ning, and R. Altermus, "Optically stimulated luminescent glass optical fiber dosimeter," Radiat. Prot. Dosim. **101**, 23–26 (2002).
[19]B. L. Justus, P. Falkenstein, A. L. Huston, M. C. Plazas, H. Ning, and R. W. Miller, "Elimination of Cerenkov interference in a fibre-optic-coupled radiation dosimeter," Radiat. Prot. Dosim. **120**, 20–23 (2006).
[20]L. A. Benevides, A. L. Huston, B. L. Justus, P. Falkenstein, L. F. Brateman, and D. E. Hintenlang, "Characterization of a fiber-optic-coupled radioluminescent detector for application in the mammography energy range," Med. Phys. **34**, 2220–2227 (2007).
[21]D. E. Hyer, R. F. Fisher, and D. E. Hintenlang, "Characterization of a water-equivalent fiber-optic coupled dosimeter for use in diagnostic radiology," Med. Phys. **36**, 1711–1176 (2009).
[22]ICRU, "Stopping powers for electrons and positrons," ICRU Report No. 37 (International Commission on Radiation Units and Measurements, Bethesda, MD, 1984).
[23]R. W. Miller, H. Ning, B. Justus, A. Huston, P. Falkenstein, G. Li, H. Xie, and C. N. Coleman, "Clinical implementation of a real-time fiber optic dosimetry system," Int. J. Radiat. Oncol., Biol., Phys. **63**, S494 (2005).